

DRAFT VERSION MAY 8, 2024
Typeset using L^AT_EX **preprint2** style in AAS_{TeX}631

New 511 keV line data provides strongest sub-GeV dark matter constraints

PEDRO DE LA TORRE LUQUE,^{1,2,3} SHYAM BALAJI,⁴ AND JOSEPH SILK^{5,6,7}

¹*Departamento de Física Teórica, M-15, Universidad Autónoma de Madrid, E-28049 Madrid, Spain*

²*Instituto de Física Teórica UAM-CSIC, Universidad Autónoma de Madrid, C/ Nicolás Cabrera, 13-15, 28049 Madrid, Spain*

³*The Oskar Klein Centre, Department of Physics, Stockholm University, Stockholm 106 91, Sweden*

⁴*Physics Department, King's College London, Strand, London, WC2R 2LS, United Kingdom*

⁵*Institut d'Astrophysique de Paris, UMR 7095 CNRS & Sorbonne Université, 98 bis boulevard Arago, F-75014 Paris, France*

⁶*Department of Physics and Astronomy, The Johns Hopkins University, 3400 N. Charles Street, Baltimore, MD 21218, U.S.A.*

⁷*Beecroft Institute for Particle Astrophysics and Cosmology, University of Oxford, Keble Road, Oxford OX1 3RH, U.K.*

ABSTRACT

We explore the 511 keV emission associated to sub-GeV dark matter (DM) particles that can produce electron-positron pairs and form positronium after thermalizing. We use ~ 16 yr of SPI data from INTEGRAL to constrain DM properties, considering the full positron propagation and losses, and the free electron density drop away from the Galactic plane. We show that the predicted longitude and latitude profiles vary significantly for different DM masses, unlike previous assumptions, and obtain the strongest limits on sub-GeV DM (from the MeV to a few GeV) so far, excluding cross-sections down to $\langle\sigma v\rangle \lesssim 10^{-32} \text{ cm}^3 \text{ s}^{-1}$ for $m_\chi \sim 1 \text{ MeV}$ and $\langle\sigma v\rangle \lesssim 10^{-26} \text{ cm}^3 \text{ s}^{-1}$ for $m_\chi \sim 5 \text{ GeV}$ and lifetimes up to $\tau \gtrsim 10^{29} \text{ s}$ ($m_\chi \sim 1 \text{ MeV}$) and $\tau \gtrsim 10^{27} \text{ s}$ ($m_\chi \sim 5 \text{ GeV}$) for the typical Navarro-Frenk-White DM profile. Our derived limits are robust within a factor of a few due to systematic uncertainties.

1. INTRODUCTION

The 511 keV γ -ray line from the galactic bulge indicates e^+e^- annihilation into $\gamma\gamma$ via positro-

nium in the interstellar medium (ISM). This line has been measured by SPI on INTEGRAL (Siegert et al. 2016) and COSI (Kierans et al. 2020), and reviewed in Prantzos et al. (2011); Kierans et al. (2019); Siegert (2023). The line has disk and bulge components, with the bulge component being narrow, bright and centered at the galactic center (GC), with a flux of $\sim 10^{-3}$

pedro.delatorreluque@fysik.su.se

shyam.balaji@kcl.ac.uk

silk@iap.fr

$\text{cm}^{-2} \text{s}^{-1}$ (Siegert et al. 2016). This has been used to constrain possible positron sources, such as isotopes from stars (Prantzos et al. 2011; Bartels et al. 2018), low-mass X -ray binaries (Bartels et al. 2018) or neutron star mergers (Fuller et al. 2019).

The bulge positrons could also come from dark matter (DM), which is abundant near the GC. This possibility has been explored, at least, since Boehm et al. (2004b). However, not all DM models work. For example, DM decay does not fit the signal shape Vincent et al. (2012); Ascasibar et al. (2006). Moreover, the positron injection energy must be around MeV scale Beacom et al. (2005); Boehm & Uwer (2006); Beacom & Yüksel (2006); Boehm (2009), which implies that the DM mass must be below some tens of MeV, unless there are intermediate steps in the annihilation. Such a low DM mass was thought to be inconsistent with cosmology, but recent studies have shown that it can be compatible with observations if there is also neutrino injection from DM annihilation in the early universe Escudero (2019); Sabti et al. (2020). We use these new findings to motivate study of light DM scenarios that may produce the 511 keV line.

Vincent et al. (2012) showed that the DM annihilation rate needed to explain the 511 keV line emission in the bulge (from ~ 8 years of SPI data in a 5 keV bin), was approximately

$$\langle\sigma v\rangle_{511} \simeq 5 \times 10^{-31} \left(\frac{m_\chi}{3 \text{ MeV}} \right)^2 \frac{\text{cm}^3}{\text{s}}, \quad (1)$$

for a Navarro-Frenk-White (NFW) profile DM density distribution for the best fit parameters in Vincent et al. (2012).

However, the previous studies have assumed that positrons follow the DM distribution and have ignored positron propagation in the Galaxy, that depends on their energy, E (with $D(E) \propto E^\delta$, where D is the diffusion coefficient and $\delta > 0$ means that higher energy positrons diffuse faster). This assumption was adopted

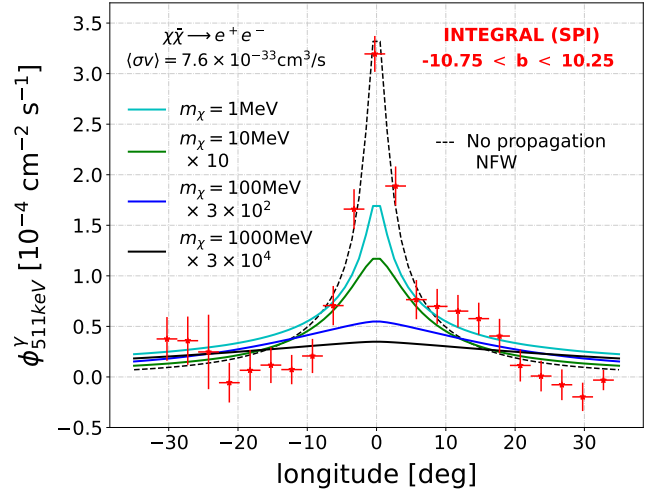


Figure 1. Diffuse 511 keV emission longitude profile in the latitude bin $-10.75^\circ < b < 10.25^\circ$ from direct DM annihilation into electron-positron pairs. We show DM masses (m_χ) ranging from 1 (cyan), 10 (green), 100 (blue) and 1000 MeV (black) respectively, and compare to the expected NFW distribution of DM. To facilitate the comparison with SPI data (shown in red), the emission for each mass is scaled by the factor indicated in the legend. We consider a typical NFW DM distribution.

since energy losses at MeV energies are dominant (Strong & Moskalenko 1998), but diffusion is still important, and leads to a 511 keV profile that changes with the DM mass, as we show in Fig. 1 and compare to the expected signal with no propagation (dashed). Moreover, the latest data from AMS-02 Aguilar et al. (2013) on secondary cosmic-rays (CRs) suggest a faster diffusion below the GeV scale (Weinrich, N. et al. 2020; Luque et al. 2021; Luque 2021; de la Torre Luque et al. 2022). Also, the interaction of charged particles with turbulence in the interstellar medium (ISM) causes energy exchange and diffusive reacceleration (Heinbach & Simon 1995; Strong & Moskalenko 1998; Cardillo 2019) (a kind of Fermi acceleration), which boosts low-energy particles to higher energies, making them diffuse faster. Therefore, we evaluate the 511 keV profile from the distribution of propagated positrons injected by DM, instead

of assuming that it follows the DM distribution. In fact, some recent works (De la Torre Luque et al. 2023a,b,c), have shown the importance of adding propagation effects in constraining sub-GeV DM.

Here, we perform a detailed evaluation of the 511 keV line emission from DM and utilize the non-compatibility of these signals with the observed 511 keV line morphology, to constrain the DM annihilation/decay cross-section and lifetime for the kinematically accessible channels. In doing so, we highlight three novelties. i) We include the transport of positrons when calculating the 511 keV emission in the Galaxy. We show that the diffusion of positrons changes their spatial morphology significantly. ii) We include the fact that the free electron density drops quickly away from the Galactic Plane, which suppresses the latitude profile flux of the 511 keV emission. This is necessary for any positron source that could produce 511 keV radiation. iii) We derive strong limits on the lifetime of decaying DM. Remarkably, we find that the limits from the full SPI dataset are the most constraining ones below DM masses of ~ 1 GeV, a mass range of interest given low sensitivity in DM direct detection experiments to light DM (Cirelli et al. 2023; De la Torre Luque et al. 2023c).

2. EVALUATION OF THE 511 KEV SIGNAL

The literature assumes that the distribution of diffuse positrons from DM decay/annihilation follows the parent DM Galactic distribution. However, positrons can propagate and diffuse far from their source, changing their distribution and the profile of the observed diffuse 511 keV line in the Galaxy (Jean, P. et al. 2009). Therefore, we evaluate the DM-induced 511 keV line flux considering the full propagation of positrons, including all sources of energy losses and other effects, such as reacceleration (Seo & Ptuskin 1994; Osborne & Ptuskin

1987), triplet pair production (Gaggero et al. 2013) and in-flight annihilation (Heitler 1936). We calculate the steady-state solution for the distribution of positrons injected by DM (similar to Calore et al. (2022)) and integrate it over all possible energies.

We compare our results with more than 16 years of data from INTEGRAL/SPI, which offered the latitudinal and longitudinal profiles of the diffuse 511 keV line emission with unprecedented quality (Siegert et al. 2019).

2.1. Positron propagation

We compute the distribution and energy spectra of the positrons produced by DM annihilation/decay in the Galaxy with a customized version (De La Torre Luque 2023) of the DRAGON2 code (Evoli et al. 2017, 2018), a CR propagation code that numerically solves the full diffusion-advection-loss equation for charged particles in the Galactic environment (Ginzburg & Syrovatskii 1969). We use the same expression for the diffusion coefficient and propagation parameters as in De la Torre Luque et al. (2023c). These simulations include all the sources of energy loss, inelastic interactions, triplet pair production (Gaggero et al. 2013) and in-flight annihilation of positrons.

We simulate the channels leading to the production of e^\pm final states through the processes: $\chi\bar{\chi} \rightarrow \mu^+\mu^-, \pi^+\pi^-, e^+e^-$ for DM annihilation and $\chi \rightarrow \mu^+\mu^-, \pi^+\pi^-, e^+e^-$ for DM decay. The injection spectra dN_e/dE_e for each channel are calculated following Cirelli et al. (2021). We compute the signals from light DM from $m_\chi = m_i$ for annihilation and $m_\chi = 2m_i$ for decays, up to $m_\chi = 5$ GeV (where $i = e, \mu, \pi$), taking 3 masses per decade and a NFW DM distribution (Navarro et al. 1996), as a baseline.

Simulations are performed with a spatial resolution of ~ 150 pc, which is sufficiently fine for comparisons with SPI data and for the smooth NFW profile. We simulate electron-positron signals from DM annihilation and decay in the

range of kinetic energies from 100 eV to 10 GeV, with an energy resolution of 5%. We need to consider such low energies for reasons explained below. Lowering the minimum energy or the spatial resolution does not impact our results significantly.

2.2. 511 keV emission

Given the propagated and integrated flux of diffuse positrons in the Galaxy as a function of 3D position (x, y, z) , $\phi_e(x, y, z)$, we calculate the emission of 511 keV X -rays from a given direction by integrating over the line of sight, as

$$\frac{d\phi_\gamma^{511}}{d\Omega} = 2k_{ps} \int ds s^2 \frac{\phi_e(x_{s,b,l}, y_{s,b,l}, z_{s,b,l})}{4\pi s^2}, \quad (2)$$

where $k_{ps} = 1/4$ is the fraction of positronium decays corresponding to (singlet) para-positronium states) contributing to the 511 keV line signal, $\phi_e = \int \frac{d\phi_e}{dE} dE$ is the energy-integrated emissivity of positrons, $d\Omega = dl db \cos b$ is the solid angle element with l , b and s denoting the Galactic longitude, latitude and distance s (along the line of sight) from the Earth.

We consider that the probability of producing positronium away from the Galactic Plane depends on the positron density injected from DM and the ambient free electron density. Hence, we apply a scaling relation to the 511 keV profiles, following the vertical distribution of free electron density in the Galaxy. This is motivated by the fact that SPI observations of the latitude profile show a similar variation of the 511 keV emission as the one of the free electron density (see Section SI of the supplementary material). This scaling leads to a more conservative but realistic evaluation of the predicted 511 keV emission. For the distribution of free electrons, we use the NE2001 model (Cordes & Lazio 2003a,b), which contains the modelling of several Galactic sub-structures and is derived from a combined fit of pulsar dispersion measurements, temporal and angular broadening of

radio pulses, and intensity measurements. We consider only the vertical dependence of the electron density, since the free electron density is always much higher than the diffuse positron density in the Galactic disk. This has usually been assumed true in all the Galaxy (see, e.g. Keith & Hooper (2021); Calore et al. (2022)), however a different rate of positronium production is expected out of the Galactic plane, because of the fast reduction of free electron density when moving away from the Galactic plane. This scaling has an appreciable effect in the predicted latitude profiles, but roughly no effect on the predicted longitude profiles of the 511 keV line emission.

We adopt the scaling predicted by the NE2001 model, applying the correction proposed in Gaensler et al. (2008), where the authors found that the height of the thick disk roughly doubles to $\simeq 2$ kpc: i) a thick disk with large Galactocentric scale height (whose scaling follows a $\exp[-|z|/H_1]$ relation, where z is the Galactocentric height and the scale H_1 was found to be 1 kpc), ii) a thin, annular disk in the inner Galaxy (whose scaling decays as $\exp[-|z|/H_2]$, with $H_2 \simeq 140$ pc), and iii) a GC component. We take this scaling to be maximal at the center of the Galaxy and exponentially decays like $\exp[-|z|/H_1] + \exp[-|z|/H_2]$ at a height z , as shown in Fig. S1 of the supplementary material.

3. SUB-GEV DARK MATTER CONSTRAINTS FROM SPI DATA

In Fig. 1, we depict how predicted 511 keV line longitude profiles vary with different DM masses, specifically when directly annihilating into e^+e^- final states. Results for DM masses of 1, 10, 100, and 1000 MeV are compared to SPI data. A decreasing DM mass results in an increase of the signal normalization and a peakier profile around the GC. This effect is due to lower-energy injected positrons covering shorter distances before thermalization or annihilation,

influenced by higher gas density toward the GC. The χ^2 -profile (Fig. S2 in the supplementary material) shows that lower DM masses better match SPI’s longitude profile shape. However, the NFW profile fails to replicate the peakiness indicated by SPI measurements for DM masses above the electron mass. Only a highly peaked distribution like the Moore profile [Moore et al. \(1999\)](#) ($\gamma = 1.5$) provides a satisfactory fit, as shown in Fig. S3 (Supp. material). This emphasizes the importance of data away from central longitudes for deriving stringent DM bounds.

Similar plots for other annihilation channels ($\mu^+\mu^-$, $\pi^+\pi^-$, and direct e^+e^-) are presented in Fig. S4 (Supp. material), including the predicted longitude and latitude profiles for various DM masses. For latitude profiles, scaling the free electron density yields a profile similar to SPI’s, even at high (\sim GeV) DM masses. Considering positron annihilation in flight is crucial, impacting the distribution above or below the Galactic plane, particularly reducing emission in the plane with lower DM masses.

Additionally, as confirmed by other studies [Boehm & Fayet \(2004\)](#); [Vincent et al. \(2012\)](#), decaying DM produces a flat profile inconsistent with observations, evident in Fig. S5 (Supp. material) and supported by high χ^2 values in Fig. S2 (Supp. material) for the fit to SPI longitude and latitude profiles.

We show the bounds from SPI data and compare them to other DM constraints in Fig. 2, for DM annihilation (left panel) and decay (right panel). To derive these limits, we use a simple χ^2 fit to the SPI data, using the CURVE-FIT PYTHON package, and take the 2σ error. We show the constraints from the SPI latitude profile as a dashed curve (“SPI Lat”) and the SPI longitude profile as a solid curve (“SPI Long”). We use colour to distinguish the channel of annihilation or decay: e^+e^- (green), $\mu^+\mu^-$ (red) and $\pi^+\pi^-$ (blue). We restraint ourselves to compute the limits independently, since we ex-

pect that combining both datasets will not offer noticeable improvement and will be dominated by longitude data. In the left panel, we also compare with the limits from the e^\pm injection from DM annihilation on the CMB anisotropies, from Slatyer [Slatyer \(2016\)](#) and Lopez-Honorez et al. [Lopez-Honorez et al. \(2013\)](#), shown as dot-dashed lines (“CMB”). These limits are based on the fact that the injection of charged particles by DM during the cosmic Dark Ages must increase the residual ionization fraction, thus altering the anisotropies of the CMB. The CMB limits are weak for decaying light DM [Liu et al. \(2023a,b\)](#), unlike the case of annihilating DM. This is because DM clusters at redshifts $z \lesssim 100$, which increases the DM annihilation rate and the e^\pm injection, while the decay rate stays the same. Since the CMB bounds are weak for decaying DM, we show the stronger bound from [De la Torre Luque et al. \(2023c\)](#) (labelled “Voyager-1”) as a dot-dashed curve in the right panel. This limit comes from the fact that decaying DM results in an e^\pm cascade that can be observed by VOYAGER 1, without the solar modulation effect of the heliosphere, due to the satellite’s distance from the solar system.

We show the strong bounds from [De la Torre Luque et al. \(2023c\)](#), labelled as “XMM-Newton” in both panels, as dotted curves. These limits are derived from the fact that e^\pm products from an exotic DM injection of e^\pm may generate bremsstrahlung radiation and up-scatter the low-energy Galactic photon fields via the inverse Compton process, producing a broad emission from X-ray to γ -ray energies observable by XMM-NEWTON, which measured X-rays in galactocentric rings around the GC. These limits include best-fit CR propagation and diffusion parameters and represented the strongest astrophysical constraints for this mass range of DM of 1 MeV to a few GeV and surpass cosmological bounds across a wide range of masses.

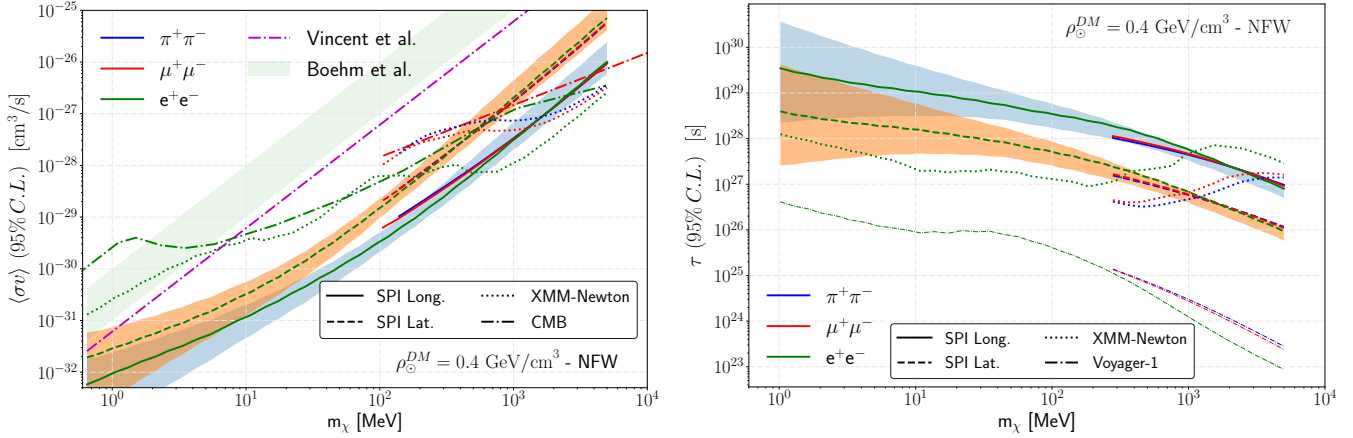


Figure 2. Comparison of the 95% confidence bounds on annihilating (left panel) or decaying (right panel) DM derived in this work (thick dashed for SPI LAT and solid lines for SPI LONG, respectively) with other existing constraints. We show the CMB bounds from Slatyer [Slatyer \(2016\)](#) and Lopez-Honorez et al. [Lopez-Honorez et al. \(2013\)](#) (dot-dashed line), the bounds from XMM NEWTON [De la Torre Luque et al. \(2023c\)](#) (dotted line), the previous 511 keV line bounds from Vincent et. al [Vincent et al. \(2012\)](#) (red dashed line) and from VOYAGER 1 [De la Torre Luque et al. \(2023c\)](#) (dot-dashed line). In both panels, we assume a NFW DM density distribution and show the $\pi^+\pi^-$ (blue), $\mu^+\mu^-$ (red) and e^+e^- (green) channels, respectively. Uncertainties in our limits from the propagation setup employed are shown as an orange and a blue band, for the latitude and longitude profiles, respectively.

We show the bounds from [Vincent et al. \(2012\)](#), also using 511 keV data from SPI after a shorter ~ 8 yr of operation. Our limits are stronger because their constraint used the spectrum of the emission at 511 keV, instead of the full profile. This, combined with the fact that we use the most constraining observations (from high longitude), explains the strength of our constraints.

In fact, we see that the SPI longitude profile provides the strongest limit on annihilating DM, excluding cross-sections of $\langle\sigma v\rangle \simeq 10^{-32} \text{ cm}^3 \text{ s}^{-1}$ at masses of around an MeV, increasing to around the thermal relic values of $\langle\sigma v\rangle \simeq 10^{-26} \text{ cm}^3 \text{ s}^{-1}$ at masses of over several GeV. This SPI longitude profile only gets surpassed by XMM-NEWTON X-ray bounds at masses $\gtrsim 700$ MeV. The CMB bounds only become more stringent than the SPI latitude profile limits at masses in excess of a few tens of GeV. Strikingly, limits derived from the SPI latitude profile are only marginally weaker (less than an order of magnitude across the en-

tire DM mass range) than the SPI longitude profile limits. This was also found in [Calore et al. \(2022\)](#). Furthermore, this bound also surpasses the other DM limits across most of the mass range considered, except XMM-NEWTON at masses over a few hundreds of MeV and CMB bounds at slightly higher mass. Finally, we also compare our limits with those derived from [Boehm et al. \(2004a\)](#) from final-state radiation (FSR) emission.

From the right panel of Fig. 2, we see once again that the SPI longitude profile provides the strongest limit on decaying DM, excluding lifetimes of $\tau \simeq 10^{29} \text{ s}$ at masses of around an MeV decreasing to around 10^{27} s at masses of over a GeV. This SPI longitude profile gets surpassed by XMM-NEWTON X-ray bounds at masses $\gtrsim 1$ GeV. Limits derived from the SPI latitude profile are about an order of magnitude weaker than the SPI longitude profile limits across the entire mass range. The next strongest limit, coming from VOYAGER 1 is significantly weaker (about three orders weaker than the SPI longi-

tude profile limits). This illustrates the power of the 511 keV line in constraining sub-GeV DM. We remark that including the free electron density scaling changes our latitude bounds by a factor of 2-3, leading to a more conservative estimate.

4. DISCUSSION AND CONCLUSION

This study investigates sub-GeV dark matter (DM) particles annihilating or decaying into standard model (SM) particles, leading to an electron-positron cascade and positronium bound-state formation. About one-fourth of these states decay into 511 keV photons, detectable by the SPI spectrometer on the INTEGRAL satellite. SPI longitude and latitude profiles are used to establish new limits on DM properties, including mass, annihilation cross-section, and decay lifetime. We enhance previous analyses by considering two previously overlooked effects: positron diffusion and propagation in the interstellar medium, and the decrease in free electron density away from the Galactic plane. These considerations significantly impact the 511 keV photon line's shape and intensity, influencing derived DM constraints. Additionally, this study presents the first constraints on decaying DM using the SPI dataset. Assuming a NFW density distribution, our limits are the strongest across the sub-GeV DM mass range (MeV to a few GeV), ruling out thermally-averaged cross-sections in the range $10^{-32} \text{ cm}^3\text{s}^{-1} \lesssim \langle\sigma v\rangle \lesssim 10^{-26} \text{ cm}^3\text{s}^{-1}$ and decay lifetimes of $10^{29} \text{ s} \lesssim \tau \lesssim 10^{27} \text{ s}$, surpassing many cosmological and astrophysical limits.

However, uncertainties persist: On the one hand, the total systematic uncertainties of the SPI data points are not totally under control, since they depend on some template models for the shape of the signal. The fact that these constraints are so sensitive to the high longitudes can be particularly affected by these systematic uncertainties, as pointed out in [De la Torre Luque et al. \(2023a\)](#), given that there

are data points indicating no flux detected at these longitudes. In that paper, we found that constraining ourselves to the inner 20° instead (expected to be less affected by the detector's systematic uncertainties) leads to a factor of 2 weaker limit. On the other hand, we expect that uncertainties in the CR propagation setup affect the predicted flux of positrons from DM. Ref [De la Torre Luque et al. \(2023c\)](#) demonstrated that the main factors affecting the flux of positrons produced from sub-GeV DM are the halo height and the Àlfven speed (controlling the level of reacceleration). Therefore, we have built a pessimistic and optimistic propagation setups to compute the uncertainty bands shown in Fig. 2. The pessimistic setup features the scenario with very slow diffusion, where the halo height is set to $H = 3 \text{ kpc}$ (given that the lower the halo height, the lower the positron flux ([De la Torre Luque et al. 2023c](#)), we take a very small value compared to the typical values obtained in CR analyses), keeping the ratio of the normalization of the diffusion coefficient to the halo height (H/D_0) to the value that reproduces CR secondary ratios at Earth. In addition, we assume no reacceleration (i.e. $V_A = 0 \text{ km/s}$). In the optimistic case, we set $V_A = 40 \text{ km/s}$ and $H = 16 \text{ kpc}$. As we observe from Fig. 2, at low masses, uncertainties in reacceleration make our limits be uncertain by up to an order of magnitude, while at high masses the effect of reacceleration is minor and uncertainties in the halo height make our limits uncertain by a factor of up to 2-3, compatible with what was also found in [De la Torre Luque et al. \(2023c\)](#). Effects like strong convection or winds near the Galactic Center could also alter the positron spectra, but accurate estimation with current data is challenging. On top of this, we have checked that these limits do not change by more than a factor of a few using a cuspier DM distribution than the NFW. An Einasto profile is expected to slightly strengthen these limits,

given that it results in more DM density at intermediate longitudes. Following the same reasoning, the use of a more cored profile, like the Isothermal one, could worsen the limits. However, even with these uncertainties, our results show that the 511 keV line provide the strongest astrophysical bounds so far, specially on the decay lifetime in the full MeV-to-GeV range.

Furthermore, for a NFW DM profile, we find that DM masses above a few tens of MeV can not reproduce the high peak intensity in the bulge (i.e. at the central longitudes), therefore, being unable to explain the 511 keV profile, even in the case of DM annihilation (in agreement with [Beacom & Yuksel \(2006\)](#)). Additionally, while DM predicts a totally symmetric profile, the SPI data seem to indicate that there is some asymmetry in the emission. However, this asymmetry is not significant above $\sim 2\sigma$, and may be also affected by systematic uncertainties in the measurements.

Future data from the COSI [Siegert et al. \(2020\)](#) with improved spatial resolution would provide insights into processes and structures producing the 511 keV line in the Milky Way. Additionally, testing these DM scenarios by characterizing diffuse MeV-scale γ -ray emission from the Milky Way halo, using proposed γ -ray telescopes like AMEGO [McEnery et al. \(2019\)](#) or e-ASTROGAM [De Angelis et al. \(2018\)](#),

could provide useful background models and further strengthen bounds on sub-GeV DM.

5. ACKNOWLEDGEMENTS

We are grateful to Pierluca Carenza, Marco Cirelli, Daniele Gaggero, Dan Hooper, Jordan Koechler, Tim Linden, Pierrick Martin and Thomas Siebert for useful discussions. SB is supported by the STFC under grant ST/X000753/1. P.D.L. was supported by the European Research Council under grant 742104 and the Swedish National Space Agency under contract 117/19 during the first stages of this work. P.D.L. is currently supported by the Juan de la Cierva JDC2022-048916-I grant, funded by MCIU/AEI/10.13039/501100011033 European Union "NextGenerationEU"/PRTR. The work of P.D.L. is now supported by the grants PID2021-125331NB-I00 and CEX2020-001007-S, both funded by MCIN/AEI/10.13039/501100011033 and by "ERDF A way of making Europe". P.D.L. also acknowledge the MultiDark Network, ref. RED2022-134411-T. This project used computing resources from the Swedish National Infrastructure for Computing (SNIC) under project Nos. 2021/3-42, 2021/6-326, 2021-1-24 and 2022/3-27 partially funded by the Swedish Research Council through grant no. 2018-05973.

REFERENCES

- Ackermann, M., et al. 2017, *The Astrophysical Journal*, 840, 43, doi: [10.3847/1538-4357/aa6cab](#)
- Aguilar, M., et al. 2013, *Phys. Rev. Lett.*, 110, 141102, doi: [10.1103/PhysRevLett.110.141102](#)
- Ascasibar, Y., et al. 2006, *Mon. Not. Roy. Astron. Soc.*, 368, 1695, doi: [10.1111/j.1365-2966.2006.10226.x](#)
- Balaji, S., et al. 2023, *JCAP*, 08, 063, doi: [10.1088/1475-7516/2023/08/063](#)
- Bartels, R., et al. 2018, *Mon. Not. Roy. Astron. Soc.*, 480, 3826, doi: [10.1093/mnras/sty2135](#)
- Beacom, J. F., Bell, N. F., & Bertone, G. 2005, *Phys. Rev. Lett.*, 94, 171301, doi: [10.1103/PhysRevLett.94.171301](#)
- Beacom, J. F., & Yuksel, H. 2006, *Phys. Rev. Lett.*, 97, 071102, doi: [10.1103/PhysRevLett.97.071102](#)
- Boehm, C. 2009, *New Journal of Physics*, 11, 105009, doi: [10.1088/1367-2630/11/10/105009](#)
- Boehm, C., Enßlin, T. A., & Silk, J. 2004a, *Journal of Physics G: Nuclear and Particle Physics*, 30, 279–285, doi: [10.1088/0954-3899/30/3/004](#)

- Boehm, C., & Fayet, P. 2004, Nucl. Phys. B, 683, 219, doi: [10.1016/j.nuclphysb.2004.01.015](https://doi.org/10.1016/j.nuclphysb.2004.01.015)
- Boehm, C., & Uwer, P. 2006, Revisiting Bremsstrahlung emission associated with Light Dark Matter annihilations.
<https://arxiv.org/abs/hep-ph/0606058>
- Boehm, C., et al. 2004b, Phys. Rev. Lett., 92, 101301, doi: [10.1103/PhysRevLett.92.101301](https://doi.org/10.1103/PhysRevLett.92.101301)
- Calore, F., et al. 2022, Phys. Rev. D, 105, 063026, doi: [10.1103/PhysRevD.105.063026](https://doi.org/10.1103/PhysRevD.105.063026)
- Cardillo, M. 2019, Galaxies, 7, 49, doi: [10.3390/galaxies7020049](https://doi.org/10.3390/galaxies7020049)
- Cirelli, M., et al. 2021, Phys. Rev. D, 103, 063022, doi: [10.1103/PhysRevD.103.063022](https://doi.org/10.1103/PhysRevD.103.063022)
- . 2023, JCAP, 07, 026, doi: [10.1088/1475-7516/2023/07/026](https://doi.org/10.1088/1475-7516/2023/07/026)
- Cordes, J. M., & Lazio, T. J. W. 2003a, NE2001. II. Using Radio Propagation Data to Construct a Model for the Galactic Distribution of Free Electrons.
<https://arxiv.org/abs/astro-ph/0301598>
- . 2003b, NE2001.I. A New Model for the Galactic Distribution of Free Electrons and its Fluctuations.
<https://arxiv.org/abs/astro-ph/0207156>
- De Angelis, A., et al. 2018, Journal of High Energy Astrophysics, 19, 1–106, doi: [10.1016/j.jheap.2018.07.001](https://doi.org/10.1016/j.jheap.2018.07.001)
- De La Torre Luque, P. 2023, DRAGON2_Optimized_DM&Antinuclei, Zenodo, doi: [10.5281/zenodo.10076728](https://doi.org/10.5281/zenodo.10076728)
- De la Torre Luque, P., Balaji, S., & Carenza, P. 2023a, Accepted in PRD.
<https://arxiv.org/abs/2307.13731>
- . 2023b, To appear as letter in PRD.
<https://arxiv.org/abs/2307.13728>
- De la Torre Luque, P., Balaji, S., & Koechler, J. 2023c, Accepted in The Astrophysical Journal.
<https://arxiv.org/abs/2311.04979>
- de la Torre Luque, P., et al. 2022, JCAP, 07, 008, doi: [10.1088/1475-7516/2022/07/008](https://doi.org/10.1088/1475-7516/2022/07/008)
- Ema, Y., Sala, F., & Sato, R. 2021, The European Physical Journal C, 81, doi: [10.1140/epjc/s10052-021-08899-y](https://doi.org/10.1140/epjc/s10052-021-08899-y)
- Escudero, M. 2019, JCAP, 02, 007, doi: [10.1088/1475-7516/2019/02/007](https://doi.org/10.1088/1475-7516/2019/02/007)
- Evoli, C., et al. 2017, JCAP, 02, 015, doi: [10.1088/1475-7516/2017/02/015](https://doi.org/10.1088/1475-7516/2017/02/015)
- . 2018, JCAP, 07, 006, doi: [10.1088/1475-7516/2018/07/006](https://doi.org/10.1088/1475-7516/2018/07/006)
- Foëx, G., et al. 2012, Astronomy & Astrophysics, 546, A106, doi: [10.1051/0004-6361/201218973](https://doi.org/10.1051/0004-6361/201218973)
- Fuller, G. M., et al. 2019, Phys. Rev. Lett., 122, 121101, doi: [10.1103/PhysRevLett.122.121101](https://doi.org/10.1103/PhysRevLett.122.121101)
- Gaensler, B. M., et al. 2008, Publications of the Astronomical Society of Australia, 25, 184–200, doi: [10.1071/as08004](https://doi.org/10.1071/as08004)
- Gaggero, D., Serpico, P. D., & Bonnivard, V. 2013, in 33rd International Cosmic Ray Conference, 0361
- Ginzburg, V. L., & Syrovatskii, S. I. 1969, The origin of cosmic rays (Gordon & Breach Publishing Group)
- Gondolo, P., & Silk, J. 1999, Physical Review Letters, 83, 1719–1722, doi: [10.1103/physrevlett.83.1719](https://doi.org/10.1103/physrevlett.83.1719)
- Heinbach, U., & Simon, M. 1995, ApJ, 441, 209, doi: [10.1086/175350](https://doi.org/10.1086/175350)
- Heitler, W. 1936, International Series of Monographs on Physics, Vol. 5, The quantum theory of radiation (Oxford: Oxford University Press)
- Jean, P., et al. 2009, A&A, 508, 1099, doi: [10.1051/0004-6361/200809830](https://doi.org/10.1051/0004-6361/200809830)
- Keith, C., & Hooper, D. 2021, Phys. Rev. D, 104, 063033, doi: [10.1103/PhysRevD.104.063033](https://doi.org/10.1103/PhysRevD.104.063033)
- Kierans, C. A., et al. 2019, Positron Annihilation in the Galaxy.
<https://arxiv.org/abs/1903.05569>
- . 2020, Astrophys. J., 895, 44, doi: [10.3847/1538-4357/ab89a9](https://doi.org/10.3847/1538-4357/ab89a9)
- Lacroix, T. 2018, Astron. Astrophys., 619, A46, doi: [10.1051/0004-6361/201832652](https://doi.org/10.1051/0004-6361/201832652)
- Liu, H., et al. 2023a, Phys. Rev. D, 108, 043530, doi: [10.1103/PhysRevD.108.043530](https://doi.org/10.1103/PhysRevD.108.043530)
- . 2023b, Phys. Rev. D, 108, 043531, doi: [10.1103/PhysRevD.108.043531](https://doi.org/10.1103/PhysRevD.108.043531)
- Lopez-Honorez, L., et al. 2013, JCAP, 07, 046, doi: [10.1088/1475-7516/2013/07/046](https://doi.org/10.1088/1475-7516/2013/07/046)
- Luque, P. D. L. T. 2021, JCAP, 11, 018, doi: [10.1088/1475-7516/2021/11/018](https://doi.org/10.1088/1475-7516/2021/11/018)
- Luque, P. D. L. T., et al. 2021, JCAP, 07, 010, doi: [10.1088/1475-7516/2021/07/010](https://doi.org/10.1088/1475-7516/2021/07/010)
- McEnery, J., et al. 2019, All-sky Medium Energy Gamma-ray Observatory: Exploring the Extreme Multimessenger Universe.
<https://arxiv.org/abs/1907.07558>
- Moore, B., et al. 1999, The Astrophysical Journal, 524, L19–L22, doi: [10.1086/312287](https://doi.org/10.1086/312287)

- Navarro, J. F., Frenk, C. S., & White, S. D. 1996, *Astrophys. J.*, 462, 563, doi: [10.1086/177173](https://doi.org/10.1086/177173)
- Navarro, J. F., et al. 2004, *Mon. Not. Roy. Astron. Soc.*, 349, 1039, doi: [10.1111/j.1365-2966.2004.07586.x](https://doi.org/10.1111/j.1365-2966.2004.07586.x)
- Osborne, J., & Ptuskin, V. 1987, in *International Cosmic Ray Conference*, Vol. 2, 218
- Prantzos, N., et al. 2011, *Rev. Mod. Phys.*, 83, 1001, doi: [10.1103/RevModPhys.83.1001](https://doi.org/10.1103/RevModPhys.83.1001)
- Sabti, N., et al. 2020, *JCAP*, 01, 004, doi: [10.1088/1475-7516/2020/01/004](https://doi.org/10.1088/1475-7516/2020/01/004)
- Seo, E.-S., & Ptuskin, V. S. 1994, *ApJ*, 431, 705
- Siegert, T. 2023, *Astrophysics and Space Science*, 368, doi: [10.1007/s10509-023-04184-4](https://doi.org/10.1007/s10509-023-04184-4)
- Siegert, T., et al. 2016, *Astron. Astrophys.*, 586, A84, doi: [10.1051/0004-6361/201527510](https://doi.org/10.1051/0004-6361/201527510)
- . 2019, *A&A*, 627, A126, doi: [10.1051/0004-6361/201833856](https://doi.org/10.1051/0004-6361/201833856)
- . 2020, *The Astrophysical Journal*, 897, 45, doi: [10.3847/1538-4357/ab9607](https://doi.org/10.3847/1538-4357/ab9607)
- Slatyer, T. R. 2016, *Phys. Rev. D*, 93, 023527, doi: [10.1103/PhysRevD.93.023527](https://doi.org/10.1103/PhysRevD.93.023527)
- Spekkens, K., & Giovanelli, R. 2005, *Astron. J.*, 129, 2119, doi: [10.1086/429592](https://doi.org/10.1086/429592)
- Strong, A. W., & Moskalenko, I. V. 1998, *The Astrophysical Journal*, 509, 212, doi: [10.1086/306470](https://doi.org/10.1086/306470)
- Vegetti, S., & Vogelsberger, M. 2014, *Mon. Not. Roy. Astron. Soc.*, 442, 3598, doi: [10.1093/mnras/stu1284](https://doi.org/10.1093/mnras/stu1284)
- Vincent, A. C., Martin, P., & Cline, J. M. 2012, *JCAP*, 04, 022, doi: [10.1088/1475-7516/2012/04/022](https://doi.org/10.1088/1475-7516/2012/04/022)
- Walker, S. A., et al. 2012, *Mon. Not. Roy. Astron. Soc.*, 424, 1826, doi: [10.1111/j.1365-2966.2012.21282.x](https://doi.org/10.1111/j.1365-2966.2012.21282.x)
- Weinrich, N., et al. 2020, *A&A*, 639, A131, doi: [10.1051/0004-6361/202037875](https://doi.org/10.1051/0004-6361/202037875)

6. HEIGHT SCALE OF THE FREE ELECTRON DENSITY

As explained above, in order to consider that different regions of the Galaxy will have a different rate (probability) of positronium formation, that also depends on the distribution of the ambient (free) electrons, we consider a scaling of the 511 keV line emission following the NE2001 model [Cordes & Lazio \(2003a,b\)](#) for the free electron density distribution. In particular, we consider that the disk of the Galaxy will always contain a much larger density of free electrons in the ISM gas than diffuse positrons (i.e. there will be always more electrons available than positrons to form positronium states, thus being “saturated”, and the probability of positronium formation will mainly depend on the diffuse positron distribution). However, this assumption must be broken well above and below the disk, since the density of free electrons falls very quickly as the galactic height, z , is increased, as shown by Fig. 3. In particular, in this figure we depict the electron density distribution, at the center of the Galaxy, as a function of the Galactic height, normalized to the electron density at the GC position. This is the scale factor that we apply to our evaluations of the 511 keV line. This scaling is particularly important for very low DM masses, when the positrons lose energy very fast in the disk (but not outside the disk, since the density of gas producing these losses is much lower) and the fraction of positrons annihilated in flight (directly proportional to the gas density where the positrons propagate) becomes relevant.

This is also motivated by the fact that, as we observe from the SPI measurements of the latitude profile, the intensity of the 511 keV line decays by around one order of magnitude at 10° above or below the disk. Assuming the height of the halo is around 4-10 kpc, this means that with every ~ 0.36 -0.9 kpc, the intensity of the line decays by one order of magnitude, similar to the factor $\gtrsim 6$ that the free electron density decays every \sim kpc above or below the disk. While the predicted latitude profiles from DM appear to be quite flat (compared to the SPI data) for all the masses explored here, using this scaling we find that the predicted latitude profiles become much more similar to the shape of the SPI measurements. However, we remark that the longitude profiles predicted are roughly unaffected by this scaling.

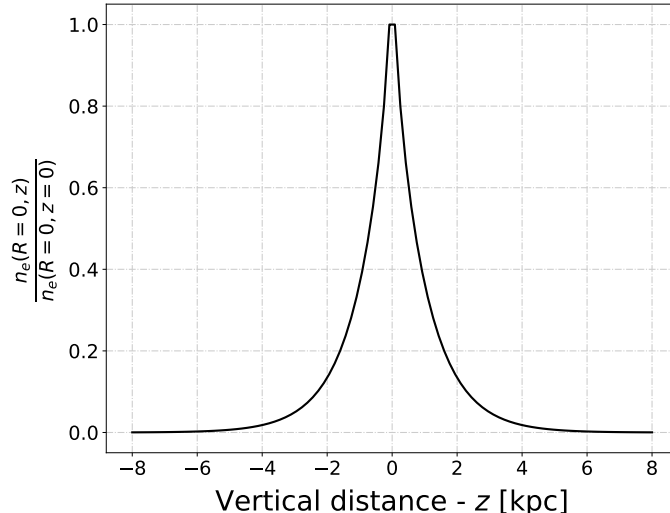


Figure 3. Vertical profile of the free electron density normalized at the Galactic Center as a function of height above the Galactic Plane z . We take this distribution from the NE2001 model [Cordes & Lazio \(2003a,b\)](#), as indicated in the text.

7. χ^2 VS DARK MATTER MASS FROM THE FITS OF SPI DATA

In this appendix, we show the χ^2 values obtained from the fits of the predicted 511 keV latitudinal and longitudinal profiles to the SPI measurements (~ 16 yr), as a function of the DM mass. The χ^2 value denotes how similar the predicted profile (for the best-fit annihilation rate) is to the one observed by SPI. Fig. 4 shows the χ^2 dependence with the DM mass for decay and annihilation, for the longitude (left panel) and latitude (right panel) profiles. First, we remark that DM decay does not lead to any good fit of the SPI measurements at all (except at high masses for the latitude profile). In turn, DM annihilation leads to profiles of the 511 keV emission that more closely resemble the data. However, while the longitude profiles favors low DM masses (in line with what was found in [Ema et al. \(2021\)](#)), the latitude profiles start to worsen below ~ 10 MeV. This misalignment in preferred mass between the latitude and longitude profile may indicate that DM is not a favoured explanation for the observed 511 keV line emission. We remind the reader that these results strongly depend on the DM density distribution, which as we mentioned earlier, we set to follow a NFW distribution, with density at Solar system position of 0.4 GeV/cm^3 .

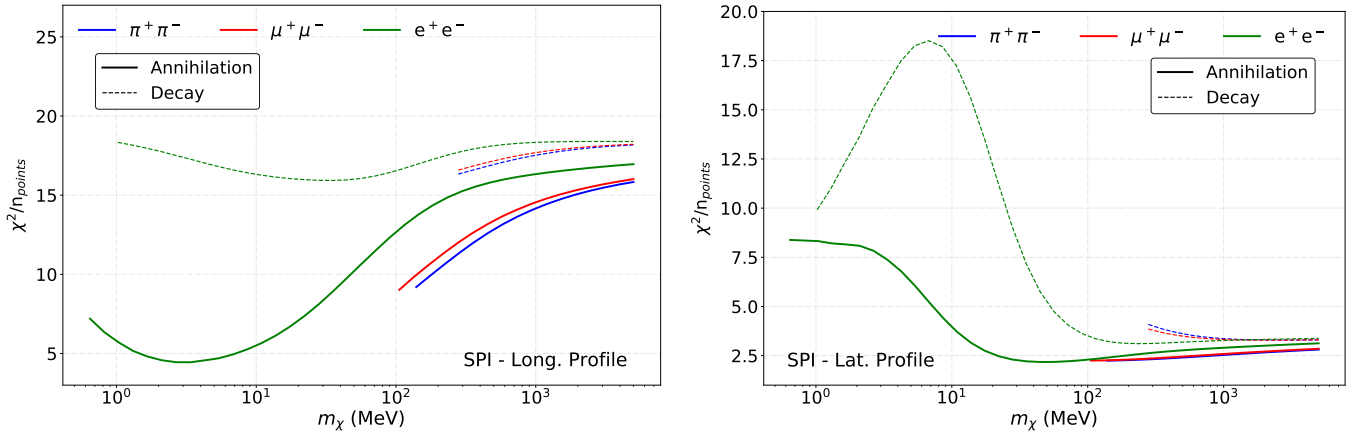


Figure 4. Reduced χ^2 (χ^2 over number of SPI data points) as function of DM mass m_χ for annihilation and decay. The left panel shows the values obtained for the analysis of the SPI longitude profile and the right panel the results for the SPI latitude profile. The channels are shown in the same colour as Fig. 2.

8. 511 KEV EMISSION PROFILES FROM COMMON GALACTIC DARK MATTER DENSITY DISTRIBUTIONS

In this appendix, we report a comparison of the longitude (left panels of Fig. 5) and latitude (right panels of Fig. 5) profiles predicted for DM annihilation, assuming different standard Galactic DM distributions, for DM masses of 10 and 100 MeV. In particular, we show the predictions obtained for the NFW profile (cyan lines), a contracted NFW profile (c-NFW), like the one that provides the best-fit to the Galactic Center Excess (GCE) [Ackermann et al. \(2017\)](#), which has a slope of $\gamma = 1.25$ (green lines), a Moore profile [Moore et al. \(1999\)](#), which has a slope of $\gamma = 1.5$ (blue lines), and a cuspy profile, as an example of a distribution that accounts for spikes formed around the central black hole Sgr A*, taken from [Gondolo & Silk \(1999\)](#); [Lacroix \(2018\)](#); [Balaji et al. \(2023\)](#) (black lines).

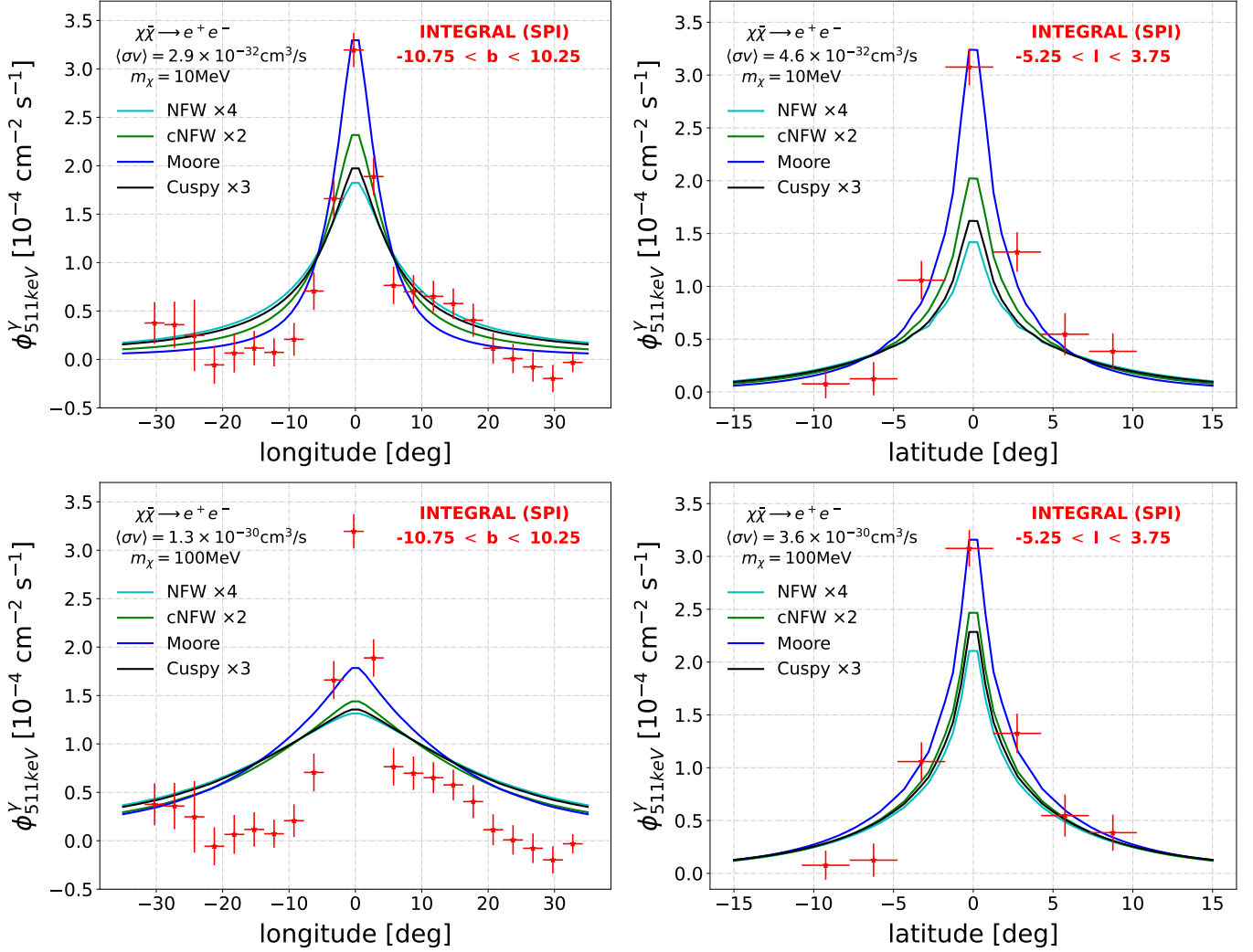


Figure 5. Comparison of the predicted diffuse 511 keV line emission from a low-mass DM particle of mass $m_\chi = 10 \text{ MeV}$ (top panels) and $m_\chi = 100 \text{ MeV}$ (bottom panels) annihilating into electron-positron pairs for different DM density profiles. The left panels are the predicted longitude profiles, for latitude bin $-10.75^\circ < b < 10.25^\circ$ while the right panels are the latitude profile, for a longitude bin of $-5.25^\circ < l < 3.75^\circ$. We fix the annihilation rate to the values shown in the plots and scale the profiles for different masses to facilitate the comparison with the SPI data. We show the NFW profile (cyan), contracted NFW (green), Moore (blue) and cuspy DM profiles.

We defer the full study of the compatibility of the different DM distributions with the SPI observations to a future work. However, this comparison allows us to see how the profiles are sensitive to the different choice of the Galactic DM distribution. In particular, we see that profiles that are not very steep (with slope $\gamma \lesssim 1.25$) are not able to produce a good simultaneous fit to the longitudinal and latitudinal SPI profiles for DM mass exceeding an MeV. However, a steeper profile would be able to provide relatively satisfactory fits for MeV masses. However, we remark that a high slope, like that adopted in the Moore profile, is already in tension with some astrophysical observations. This is because it can predict too much DM in the inner regions of galaxies and galaxy clusters to comply with rotation curve observations [Spekkens & Giovanelli \(2005\)](#), X-ray observations of galactic clus-

ters Walker et al. (2012), gravitational lensing observations Foëx et al. (2012); Vegetti & Vogelsberger (2014) and N-body simulations of Λ CDM halos Navarro et al. (2004). In general, this leads to the conclusion that DM cannot be the dominant source of positrons in the Galaxy, but, instead, it is expected that a combination of different sources is producing the peaked 511 keV emission profiles that SPI observes.

9. ANNIHILATION AND DECAY PROFILES FOR DIFFERENT CHANNELS

In this appendix, we report the predicted latitude and longitude profiles of the 511 keV emission from DM decay and annihilation. In particular, we show in Fig. 6 a comparison of profiles obtained assuming DM annihilation through the $\mu^+\mu^-$ (top panels), $\pi^+\pi^-$ (middle panel) and direct e^+e^- (bottom panels) channels for different DM masses (from twice the mass of the final state, around 100 MeV, to 5 GeV, in the case of the $\pi^+\pi^-$ and $\mu^+\mu^-$ channels, and from 1 MeV to 1 GeV for the direct e^+e^- channel). The left panels illustrate the predicted longitude profiles of the 511 keV emission and the right panels the predicted latitude profiles. These comparisons allow us to see that the data points corresponding to the higher longitude and latitude angles (in absolute value) are the most constraining ones, which explains why the bounds derived from this dataset are much stronger than those derived from Vincent et al. (2012) (besides the fact that these measurements are reported after double the duration of event collection). As we see, the predicted longitude profiles show a clear trend: the lower the mass of the DM particle, the more concentrated the 511 keV emission around the GC. This is expected, since a lower DM mass means a lower injection energy for the positrons, and the lower the energy of the positrons, the slower they diffuse. Hence lower energy positrons have a distribution more similar to the DM distribution (NFW in these calculations) and lose their energy closer to their injection point. As we pointed out in the previous section, the predictions from a NFW DM distribution do not lead to a 511 keV emission longitude profile as peaky as that observed by the SPI data even for the low DM masses that are accessible in the direct e^+e^- channel. In turn, as we see from the predicted latitude profiles, masses of around 100 MeV reproduce the observed SPI latitude profile quite well. We remark that this is due to the scaling that accounts for the decay of the density of free electrons away from the GC, applied for first time in this work. Without accounting for this effect, we observe that the latitude profiles become much more diffuse (i.e. flatter profiles) than what is observed. In addition, for the latitude profiles, we see that the same trend wherein lower DM mass leads to a profile more concentrated around the Galactic Plane is observed above some tens of MeV. However, once the energy loss (mainly Coulomb and ionization energy losses) becomes the dominant process during the positron propagation, the 511 keV emission at the Galactic plane starts to decay quickly, given that these particles suffer from severe energy losses and annihilation in flight losses (since this effect is proportional to the gas density, it does not affect the positrons above and below the Galactic plane). We have investigated that the minimum energy employed in these simulations (100 eV) is low enough that our results do not change appreciably for a minimum energy of 1 eV.

We show a direct comparison of the latitude profile including the density scaling (solid lines) and without including it (dashed lines) for different DM masses in Fig. 7, normalized to facilitate its visual comparison. This illustrates the importance of accounting for the density scaling to realistically evaluate the latitude profile of the 511 keV diffuse emission.

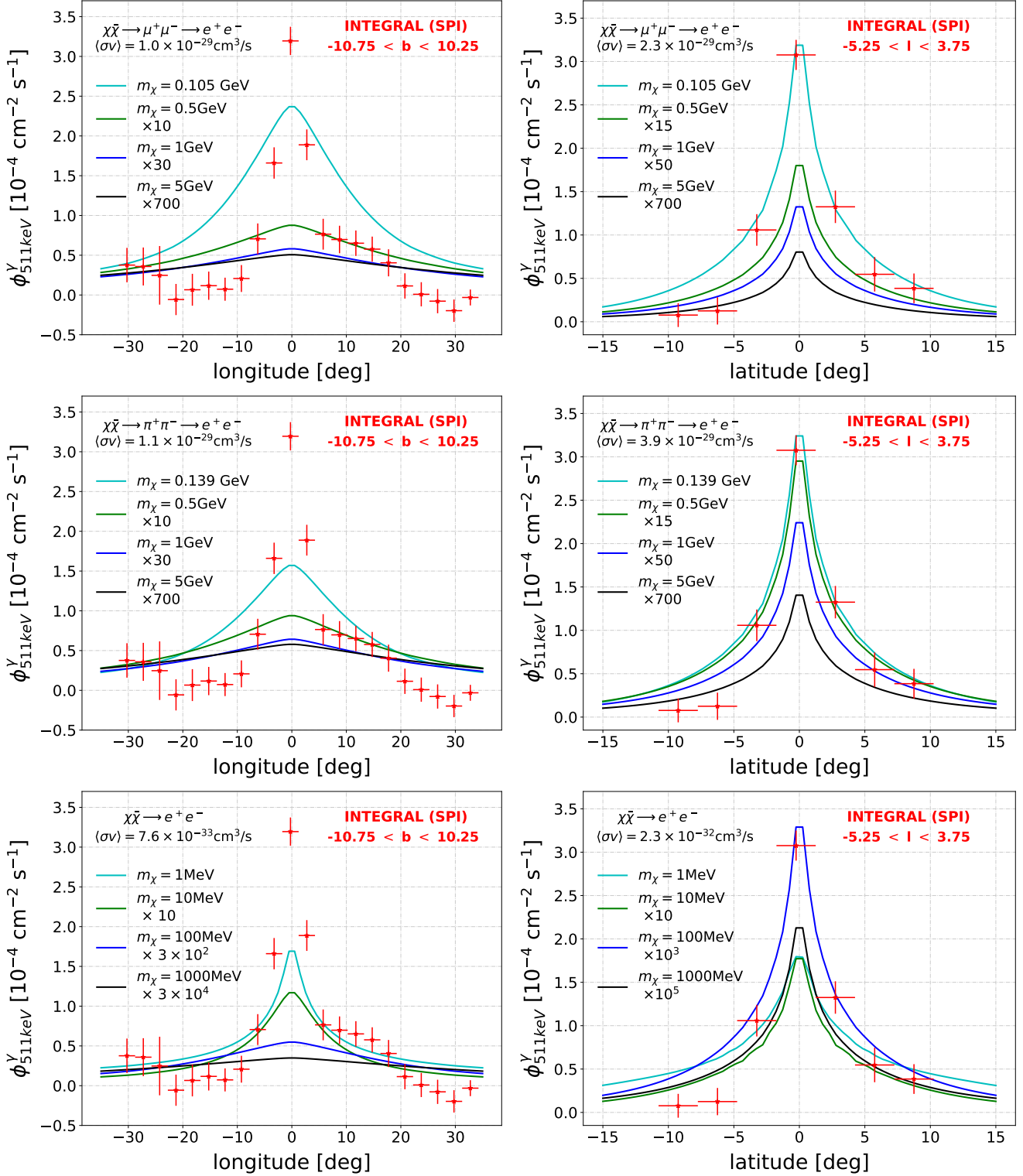


Figure 6. Comparison of the predicted longitude (left panels) and latitude (right panels) of the 511 keV emission from DM annihilation for different DM masses, through the $\mu^+\mu^-$ (top panels), $\pi^+\pi^-$ (middle panels) and direct e^+e^- (bottom panels) channels. The lowest mass for the case of the $\pi^+\pi^-$ annihilation channel is actually $m_\chi = 2m_\pi \simeq 139 \text{ MeV}$ and the minimum energy shown in the $\mu^+\mu^-$ is $m_\chi = 2m_\mu \simeq 105 \text{ MeV}$. We fix the annihilation rate to the values shown in the plots and scale the profiles for different masses to facilitate the comparison with the SPI data. The DM profiles are shown in the same colours and the left and right panels are the same latitude bins as Fig. 5.

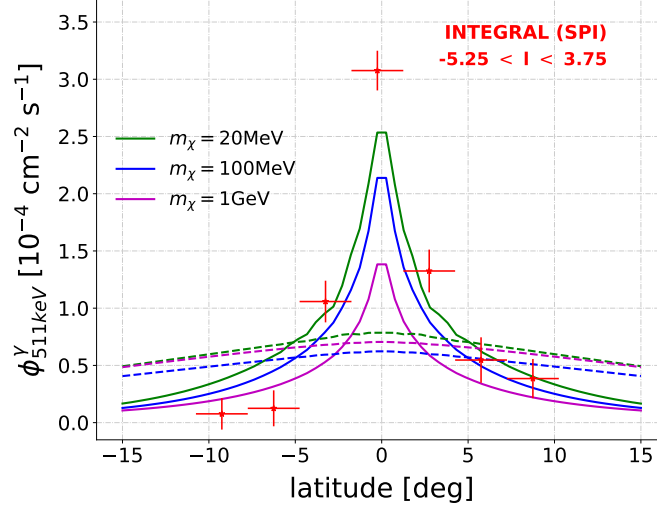


Figure 7. Comparison of the evaluated latitude profiles accounting for the scaling with the electron density (solid lines) and without considering it (dashed lines).

Finally, we show in Fig. 8 the predicted profiles from decay of DM for masses of 1 MeV to 1 GeV, in the direct e^+e^- channel. As already observed in the past, and discussed above, we observed that both the latitude and longitude profiles of the predicted 511 keV emission are much flatter (for every mass) than the ones measured by SPI, disfavouring DM decay as the main producer of the emission around the GC. This is simply due to the fact that the total positron emission from decay is proportional to the DM density, while in the case of annihilation the emission is $\propto \rho_{DM}^2$.

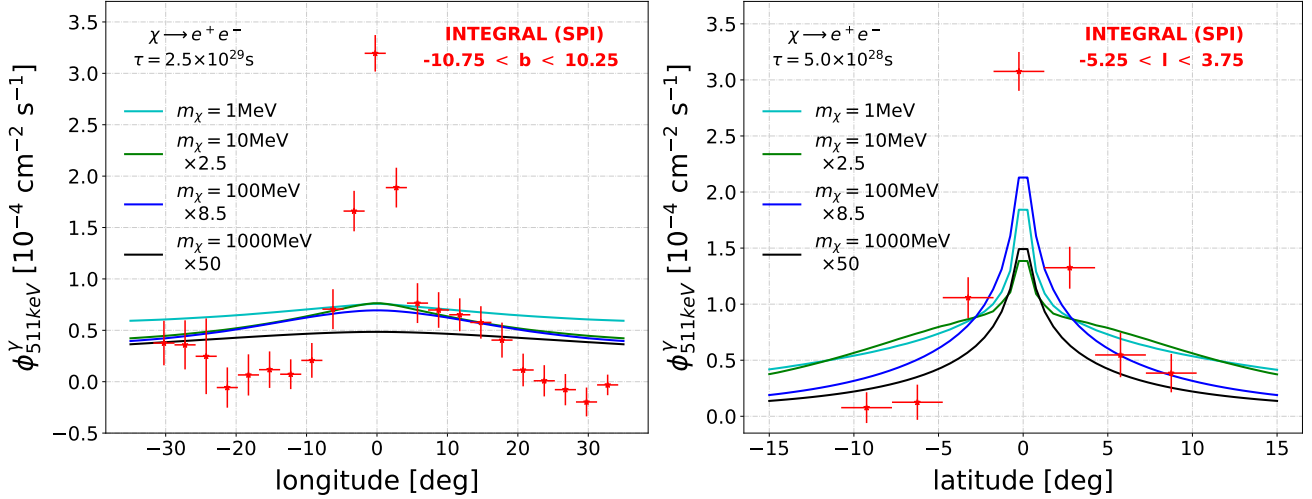


Figure 8. Similar to Fig. 6 but for the case of DM decay into the direct e^+e^- channel.